CHAPTER 8

Signals and Noise in Micromechanical Measurements

Frederick Gittes and Christoph F. Schmidt

Department of Physics, and Biophysics Research Division
University of Michigan
930 North University
Ann Arbor, Michigan 48109

I. Introduction
II. Spectral Data Analysis
    A. Interpretation of the Power Spectrum
    B. Calculation of the Power Spectrum
III. Brownian Motion of a Harmonically Bound Particle
    A. Power Spectrum of Brownian Motion
    B. Trap Calibration from a Power Spectrum
    C. Hydrodynamic Drag
IV. Noise Limitations on Micromechanical Experiments
    A. Position-Clamp Experiments
    B. Force-Clamp Experiments
    C. Dynamic Response of the Probe Interacting with a Sample
V. Sources of Instrumental Noise
    A. Noise from Electronics
    B. Other Noise Considerations
VI. Conclusions
    References

I. Introduction

A great deal is known about the static structure of the most important building blocks of life—proteins and nucleic acids—but relatively little about their motions. Intramolecular motions are, however, a central feature of the biological function of biomolecules. Thus there is great potential in new techniques that

METHODS IN CELL BIOLOGY, VOL. 55

0091-679X/98 $25.00

make it possible to study the dynamics of individual biological macromolecules. A variety of single-molecule experiments, ranging from optical tweezers and scanned-tip microscopies to single-molecule fluorescence methods, have recently begun to explore the new territory. Researchers are faced with a multitude of challenging problems, one of which is noise that sets limits on the resolution of single-molecule measurement. Instrumentation must be designed with enough stability to make measurements on nm-length scales, and a thorough understanding of the subtleties of data analysis is necessary to push the limits of detection and to avoid artifacts. In this chapter we discuss noise issues mainly in the context of optical tweezers experiments, but much of the discussion applies to other micromechanical experiments as well.

Optical tweezers, also known as laser trapping, is a micromechanical technique that is finding increasing use in a broad spectrum of experiments in biology. Optical trapping of particles uses the momentum transfer from light scattered or diffracted by an object immersed in a medium with an index of refraction different from its own (Ashkin, 1992; Ashkin *et al.*, 1986; Ashkin and Gordon, 1983). For objects much larger than the wavelength of light, for which geometric optics is a good approximation, force is imparted by refraction and reflection. For very small objects, however, the net force is proportional to the gradient of light intensity, pointing in the direction of increasing intensity. Three-dimensional trapping of particles, large or small, can be achieved at the focus of a laser beam if a strong enough gradient of intensity can be established in all directions. To achieve relatively large trapping forces, intense laser light is brought to a tight focus by a high numerical aperture (NA) lens in a microscope; for maximal force, the particles to be trapped should be roughly matched in size to the laser focus. To minimize radiation damage in biological samples, near-infrared lasers with wavelengths of approximately 1 μm are often used; these have a focus size of approximately 0.5 μm. Typical forces that can be achieved, using up to 1 W of laser power, are on the order of tens of piconewtons (pN) (Svoboda and Block, 1994a). In the simplest applications optical traps are used, literally like a pair of tweezers, to hold and move objects such as chromosomes or organelles, or to manipulate probes such as latex or glass beads. In such cases considerations of noise are largely irrelevant. In a growing number of experiments, however, laser tweezers are used in a quantitative way both to exert or measure small forces and to measure small displacements of moving objects, with sufficient resolution to study individual biological macromolecules (DNA and RNA, or proteins). Ordinary light microscopy, limited by the wavelength of light, usually cannot provide the nanometer-scale resolution needed to observe the activity of individual molecules. While spectroscopic and scattering methods do provide molecular information from a large ensemble, they cannot easily examine single-molecule motions.

Besides optical tweezers only a few recently developed techniques such as atomic force microscopy (AFM) (Radmacher *et al.*, 1995; Rugar and Hansma, 1990; Thomson *et al.*, 1996), single-molecule fluorescence microscopy (Funatsu

et al., 1995; Sase *et al.*, 1995) or near-field optical microscopy (NSOM) (Betzig and Chichester, 1993) can be used to observe the dynamics of single molecules in aqueous conditions and at room temperature. Nonimaging detection, typically with fast photodiodes, can use intense illumination in many ways to track the motion of objects with Å accuracy (Bobroff, 1986; Denk and Webb, 1990). This, for example, is how the motion of an AFM cantilever is detected (Rugar and Hansma, 1990). In the case of optical tweezers, the trapping laser beam itself can be used for position detection (Svoboda and Block, 1994a). Furthermore, the trapping forces that can be exerted are on a useful scale for single-molecule experiments, for example, to stall motor proteins (Svoboda and Block, 1994b; Svoboda *et al.*, 1993) or to stretch DNA (Smith *et al.*, 1996; Yin *et al.*, 1995).

In single-molecule optical tweezers experiments, just as with any other highly sensitive method, fighting noise in its various forms becomes of foremost importance. Noise appears in electronic components, but is also unavoidably present as the Brownian motion of the observed objects, which are typically immersed in room-temperature aqueous solutions. On the one hand unavoidable noise sources set fundamental limits to micromechanical measurements. On the other hand, one can also exploit Brownian motion to calibrate the measuring apparatus itself.

This tutorial includes the following parts: Section II, a basic discussion of power spectral analysis; Section III, a derivation of the spectral characteristics of Brownian motion of optically trapped particles and a practical recipe for the way this motion can be used to calibrate optical tweezers; Section IV, a discussion of the fundamental limits of what can be measured by optical traps or other micromechanical devices; and Section V, a discussion of instrumental design techniques that will maximize the signal-to-noise ratio.

II. Spectral Data Analysis

In the type of experiments discussed here measurements are usually taken as a set of time-domain data, for example as a series of voltage measurements corresponding to the varying light intensity detected with a photodiode (Fig. 1). Time-domain data are clearly necessary to detect singular events, but a frequency-domain description of the same data has substantial advantages for interpreting "continuous" phenomena, such as oscillations and random noise signals. Experimental or thermal noise is best characterized by its power spectrum, which is a specific frequency-domain description of an original time-domain signal. Later discussion in this chapter shows how to calculate the power spectrum numerically. Further details on the calculation of the power spectrum can be found in the literature (Press, 1992).

Conceptually, a power spectrum is obtained by passing a signal (such as a fluctuating voltage from a photodiode detector) through a set of narrow-band filters and plotting the measured intensities as a function of the filters' center

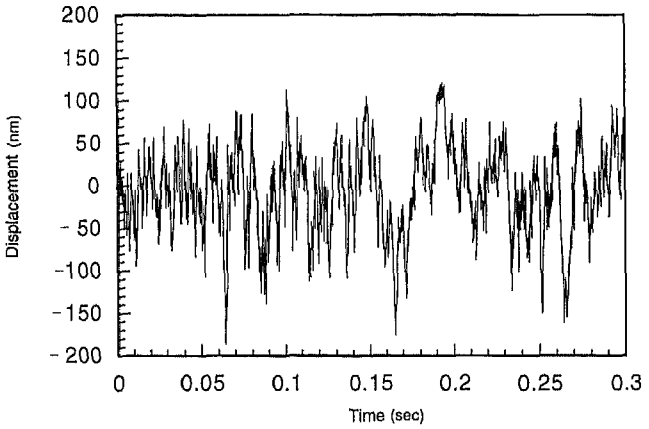

Fig. 1 Time series of data showing the Brownian motion in water of a 0.5-μm silica bead within an optical trap, at a laser power of about 6 mW in the specimen. Bead displacement was detected using an interferometric technique (Svoboda *et al.*, 1993) with a bandwidth of 50 kHz. Displacement calibration was obtained from the Lorentzian power spectrum (Fig. 4) using the methods described in this chapter.

frequencies. This process, as contrasted with a simple Fourier transform, does not preserve the total information content of the original data, as explained later. To characterize an experiment, it is necessary to know the spectral characteristics of noise, the signal, and the detection system.

A. Interpretation of the Power Spectrum

In general, going back and forth between time- and frequency-domain representations is accomplished by performing Fourier transforms. The Fourier transform of a set of real numbers (time-domain data points) gives a set of complex numbers, preserving all the information inherent in the original data. Often, however, it is more convenient to sacrifice some information content (the phases) and calculate the power spectrum or power spectral density (PSD), denoted here by $S(f)$. For practical purposes, $S(f)$ is obtained by taking the squared magnitude of the Fourier transform. This function, however, is extremely erratic: The standard deviation of each point is typically equal to its mean value. To obtain a smoother curve, many data sets must also be averaged (Press, 1992). It is this smoother curve, in the limit of infinitely many data sets, that shows the true spectral characteristics of the observed process. To understand the statistical meaning of the power spectrum, consider a set of data points, x_n: The total spread in this set of numbers is given by its variance, Var(x). One way of looking at the power spectrum is as a breakdown of this signal variance in components at frequencies f. The function $S(f)$ assigns a "power" to every frequency f, and all of the powers for nonzero frequencies add up to give exactly Var(x).

In practice, two important concepts are needed to correctly interpret $S(f)$ as calculated from a data set. These are aliasing and windowing (Press, 1992).

1. Sampling, Aliasing, and the Nyquist Frequency

If data is taken, ideally, as a series of instantaneous samples at a frequency f_s, the highest frequency component that can be unambiguously measured in the data is equal to $f_{Nyq} = f_s/2$. This f_{Nyq} is called the Nyquist frequency. A wave with frequency f_{Nyq} can have exactly one data point taken on its crests and one in its troughs. As illustrated in Fig. 2A, any wave of a frequency higher than f_{Nyq} can be erroneously interpreted as having a frequency lower than f_{Nyq}. In the power spectrum $S(f_m)$, power spectral density at frequencies above f_{Nyq} will be folded back to lower frequencies f_m below the Nyquist frequency, as shown in Fig. 2B. Such folding back of power into low frequencies is called aliasing, and the way to avoid it is to low-pass filter the signal *before* sampling it, with a cutoff frequency just at the Nyquist frequency (Horowitz and Hill, 1989).

2. Windowing

A Fourier transform of a set of N data points, used to compute the power spectrum, implicitly treats the data set as if it wrapped around periodically (i.e., mathematically x_N is implicitly followed by x_1). This can create a problem. If the data consist of, say, a pure sine wave, a narrow peak ideally is expected to appear in $S(f)$ at the wave's frequency. But the implicit wrapping around in the calculation causes the wave to appear discontinuous unless the time window is an integer multiple of the period (Fig. 3A). This discontinuity causes side lobes on the peak, as shown in Fig. 3A, which can obscure features in the power spectrum, especially close to strong lines. No perfect cure for this is possible,

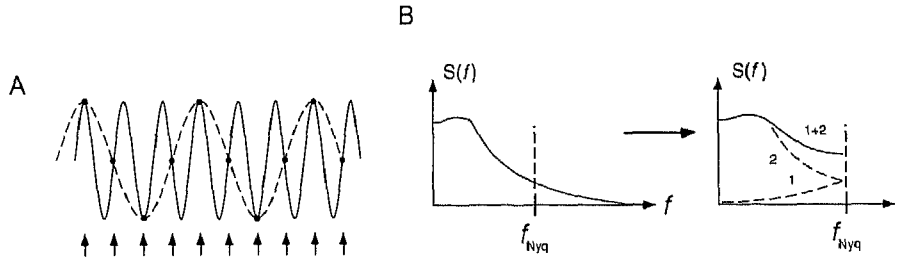

Fig. 2 (A) Schematic illustration of aliasing. A sinusoidal signal (solid curve) has a frequency that is $\frac{3}{4}$ of the sampling frequency f_s (arrows). This will falsely contribute to the power spectrum at a frequency $f_s/4$ because the sampled data (solid circles) appear as if they were produced by a wave of frequency $f_s/4$ (dotted curve). (B) For a continuous spectrum, the part of the power spectrum that continues past the Nyquist frequency $f_{Nyq} = 0.5\ f_s$ is folded back (curve 1) and added to frequencies below it (curve 2) to produce the aliased spectrum (curve 1 + 2).

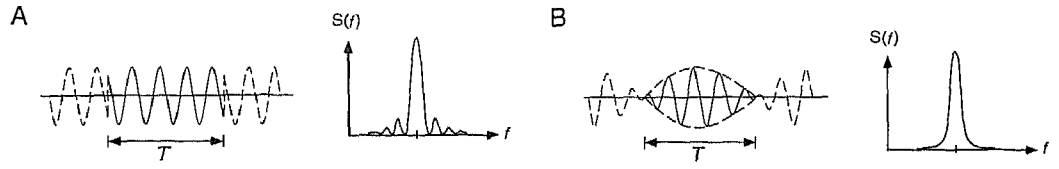

Fig. 3 Windowing of data. (A) The bottom part of the graph shows a sinusoidal signal (solid) that is measured over a time T. Outside this interval, the sinusoidal signal may continue forever. The Fourier transform algorithm, however, applied to the finite interval implicitly treats this data set as if it repeated itself with a period T (dotted curves). The artificial discontinuities and phase shifts introduced by this periodic continuation determine the width of the peak in the power spectrum (top) and create oscillations. (B) Windowing the data, that is, multiplying the data by an envelope that approaches zero at the ends of the interval (bottom), removes the oscillations in the power spectrum (top). The width cannot be reduced much.

but to minimize the effect, a "window" is applied to the data before transforming it (Fig. 3B): This means that each x_n in the data set is multiplied by some function $B(n)$ that goes to 0 at the ends of the data set. $B(n)$ should also be normalized so that the sum of all the $B(n)^2$ is equal to 1. In this way the variance of windowed data *on average* will be equal to the variance of unwindowed data (although for any particular data set, windowing changes the variance). The window shape can be optimized for specific situations but is not terribly important for relatively smooth spectra such as those discussed later. Possibilities include a parabolic hump (Welch window) or a simple triangle (Bartlett window) (Horowitz and Hill, 1989).

B. Calculation of the Power Spectrum

The following discussion shows how to obtain the power spectrum via a Fourier transform. From a set of N discrete data points x_n separated by δt, we obtain N independent fourier components $X(f_m)$, which are complex numbers given by

$$X(f_m) = \sum_{n=1}^{N} x_n e^{2\pi i n m/N}, \tag{1}$$

where each resulting $X(f_m)$ corresponds to the frequency

$$f_m = m\delta f, \quad -N/2 \leq m \leq N/2. \tag{2}$$

Before calculating $X(f_m)$ in Eq. (1), one already would have multiplied the x_n by a windowing function as described earlier. The Fourier transform in Eq. (1) is, for large data sets, greatly accelerated by use of the fast fourier transform (FFT) algorithm (Press, 1992). However, to use this algorithm, the number of data points must be an integer power of 2, a fact that should be taken into

account when collecting data. Software written to calculate power spectra may revert to much slower algorithms when the data set is not a power of 2.

The frequency resolution is determined by the total length of the measurement:

$$\delta f = \frac{1}{N\delta t}. \tag{3}$$

If, as commonly is the case, the x_n are real numbers, the components $X(f_m)$ and $X(-f_m)$ are complex conjugates, and have the same modulus. The power spectrum $S(f_m)$ is calculated from the squares of these moduli. To work with positive frequencies only, the so-called one-sided power spectrum is calculated as follows:

$$\begin{aligned} S(f_m) &= \frac{2}{N^2\delta f}|X(f_m)|^2, \\ &\quad 0 < m < N/2, \\ S(f_0 = 0) &= \frac{1}{N^2\delta f}|X(0)|^2, \\ S(f_{N/2}) &= \frac{1}{N^2\delta f}|X(f_{N/2})|^2. \end{aligned} \tag{4}$$

The highest frequency in the PSD is $f_{N/2}$, the Nyquist frequency. The power spectrum consists of $N/2$ independent numbers running from $S(0)$ to $S(f_{N/2})$, even though there were N original data points: Half the original information (concerning phases) is therefore lost in the process of calculating the PSD.

From Eqs. (1) and (4) it follows that $S(0)\delta f$ is equal to the square of the average of the measured signal x_n:

$$S(0)\delta f = \bar{x}^2, \tag{5}$$

and that the sum over the power spectrum is equal to the average of the squares of the signal data:

$$\sum_{m=0}^{N/2} S(f_m)\delta f = \overline{x^2}. \tag{6}$$

Thus we obtain the relationship to the variance as mentioned earlier:

$$\sum_{m=1}^{N/2} S(f_m)\delta f = \overline{x^2} - \bar{x}^2 = \mathrm{Var}(x). \tag{7}$$

From Eq. (7) the units of $S(f_m)$ can be read off: They are $[x]^2$/Hz. It is important to keep track of numerical factors (N and 2, etc.) so that $S(f_m)$ is properly normalized to fulfill Eq. (7). There is considerable variety in the literature and in software written to calculate power spectra. It is therefore a good idea to check the normalization by directly computing the variance of a data set (*after* multiplication by the windowing function) and comparing it with Eq. (7).

III. Brownian Motion of a Harmonically Bound Particle

For the types of microscopic systems discussed here (e.g., small optically trapped particles in a solution), the theory of Brownian motion is relatively simple because linear response theory can be used, which assumes that deviations from equilibrium positions are small. In this case, the fluctuation–dissipation theorem (Landau *et al.*, 1980; Reif, 1965) states that thermal fluctuations, such as diffusion, are governed by the same parameters that apply to larger scale motions, such as sedimentation. Furthermore, in systems with a low Reynolds number (e.g., small particles moving not too fast, in a viscous medium) viscous drag is dominant over inertial forces (Happel and Brenner, 1983).

A. Power Spectrum of Brownian Motion

A particle that can move freely in a viscous fluid performs a random walk (Brownian motion) due to the continuous bombardment by the solvent molecules (i.e., it diffuses through the fluid). In accordance with the fluctuation–dissipation theorem, the diffusional motion can be predicted once the hydrodynamic drag coefficient, γ, for steady motion is measured. This is the Einstein expression for the free diffusion coefficient D (Reif, 1965):

$$D = \frac{k_B T}{\gamma}. \tag{8}$$

In terms of D, each coordinate $x(t)$ of a diffusing particle is described by

$$Var[x] = \overline{x^2} - \bar{x}^2 = 2Dt. \tag{9}$$

For three-dimensional diffusion, squared distance from the origin grows as $r(t)^2 = 6\,Dt$ because $r^2 = x^2 + y^2 + z^2$. The random excursions of the particle from its starting point grow larger and larger as time goes by. Such random diffusion, according to Eq. (8), is proportional to the absolute temperature T.

In contrast, a particle in an optical trap feels not only random forces from solvent molecules, but also a restoring force confining it within the trap and preventing long-range diffusion. As a compromise the particle will wiggle in the trap with an average amplitude that depends on the trap strength and the temperature. Near the stationary point of the laser tweezers, the trapping force will be proportional to displacement, as for a harmonic spring. Taking, for example, a 0.5-μm silica bead, the effective spring constant can be increased from 0 to approximately 1 pN/nm by varying the laser power to a maximum of approximately 1W. The position of the particle within the trap can be monitored with Å accuracy using photodiode detection (Svoboda *et al.*, 1993). At these scales of force and distance, random Brownian motion is easily visible (Fig. 1). Thermal fluctuations are characterized by an energy on the order of $k_B T$ (k_B is Boltzmann's constant), a fact that can be used to estimate the size of Brownian motions. For

the case of a harmonic potential or linear restoring force, the prediction is precise: A particle trapped with a spring constant κ will have its position $x(t)$ vary according to a Gaussian distribution, with a displacement variance (Reif, 1965):

$$\mathrm{Var}(x) = \overline{x^2} - \bar{x}^2 = \frac{k_B T}{\kappa}. \tag{10}$$

At biological temperatures, $k_B T$ is approximately 4×10^{-21}N nm. In a trap with a stiffness of 1×10^{-2} pN/nm, according to Eq. (10), a particle moves randomly with an root mean square amplitude of approximately 20 nm. Therefore, the well-defined characteristics of Brownian motion can be exploited to calibrate the viscoelastic parameters of microscopic measurement devices (e.g., the spring constant of optical tweezers).

The power spectrum of the motion of a particle in an optical trap can also be calculated, which turns out to have a Lorentzian shape (Wax, 1954). An approximate equation of motion for the position $x(t)$ of the trapped particle is a Langevin equation. With a random thermal force $F(t)$ (see Reif, 1965 for a general discussion of Langevin equations),

$$\gamma \frac{dx}{dt} + \kappa x = F(t). \tag{11}$$

Equation (11) states a balance of forces, in which a drag force (friction times velocity) and a spring force (spring constant times displacement) are balanced by the random force $F(t)$ from the solvent bombardment. This is an approximation, with subtleties hidden in the random force and the friction coefficient (Wax, 1954), but in practice it describes the Brownian motion of micrometer-size objects in water very well. The random force $F(t)$ has an average value of 0, and its power spectrum $S_F(f)$ is a constant (i.e., it is an ideal white noise force):

$$\overline{F(t)} = 0 \text{ and } S_F(f) = |F(f)|^2 = 4\gamma k_B T. \tag{12}$$

Here $F(f)$ denotes the Fourier transform of $F(t)$. In writing $S_F(f) = |F(f)|^2$, and throughout the following derivation, we do not explicitly show the averaging needed to obtain $S_F(f)$ without encountering infinite integrals. From the Langevin Eq. (11), the power spectrum of the displacement fluctuations $S_x(f)$ of a trapped object can be derived. If the Fourier transform of $x(t)$ is $X(f)$:

$$x(t) = \int_{-\infty}^{\infty} X(f) e^{-2\pi i f t} df, \tag{13}$$

then the transform of $dx(t)/dt$ is $-2\pi i f X(f)$. The Fourier transform of both sides of the Langevin Eq. (11) gives accordingly,

$$2\pi\gamma\,(f_c - if)\,X(f) = F(f), \tag{14}$$

where we define $f_c = \kappa/2\pi\gamma$; f_c is the characteristic frequency of the trap. Both sides of Eq. (14) are complex expressions. By taking their squared modulus and writing $S_x(f) = |X(f)|^2$ and $S_F(f) = |F(f)|^2$ it will be found that

$$4\pi^2\gamma^2 (f_c^2 + f^2)S_x(f) = S_F(f). \tag{15}$$

Inserting Eq. (12), the power spectrum of $x(t)$ is

$$S_x(f) = \frac{k_B T}{\gamma\pi^2 (f_c^2 + f^2)}. \tag{16}$$

Equation (16) shows that a Lorentzian function describes how fluctuations are distributed over different frequencies f. The characteristic frequency (or corner frequency) f_c divides the Brownian motion into two regimes. For frequencies $f << f_c$, the power spectrum is approximately constant, $S_x(f) \approx S_0 = 4\gamma k_B T/\kappa^2$, which reflects the confinement of the particle. At higher frequencies, $f >> f_c$, $S_x(f)$ falls off like $1/f^2$, which is characteristic of free diffusion. Over short times the particle does not "feel" the confinement of the trap.

B. Trap Calibration from a Power Spectrum

Both the effective spring constant κ of an optical trap and the drag coefficient γ of the particle within it can be determined from a recording of Brownian motions and the calculation of their power spectrum. In practice, the time resolution of the detection device has to be better than the inverse of the corner frequency f_c. For typical trap strengths, this excludes video rate detection. For a laser power of 50 mW (at a wavelength of 1064 nm) in the specimen, and a 0.5-μm silica bead in room-temperature water, a typical spring stiffness is about 1.5×10^{-2} pN/nm, which results in a corner frequency of $f_c \approx 500$ Hz. Fig. 4 shows an experimental power spectrum in a double logarithmic plot.

The Lorentzian Eq. (16) depends on two parameters, κ and γ, which can be obtained by fitting Eq. (16) to the data by using, for example, the Levenberg-Marquardt algorithm (Press, 1992). Curve-fitting algorithms are implemented in many data graphing software packages (e.g., Origin for PC, Kaleidagraph for Mac, or XMGR for Unix). However, it is often convenient to roughly estimate these parameters by hand from a log–log plot of the Lorentzian spectrum:

1. The low-frequency portion of the log–log spectrum should be horizontal, but $S(f)$ may become large at the lowest frequencies due to drift and low-frequency vibrations. First, draw a horizontal line that ignores such effects and call its height S_0.
2. The high-frequency portion of the spectrum should be a line of slope approximately -2. Draw this line and extend it to intersect the horizontal S_0 line; this intersection determines f_c, the "corner frequency."

Once S_0 and f_c are measured, the trap stiffness can be calculated as

$$\kappa = \frac{2k_B T}{\pi S_0 f_c}, \tag{17}$$

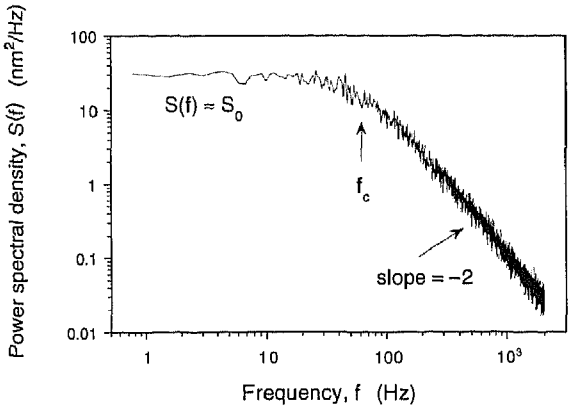

Fig. 4 The Lorentzian power spectrum of the Brownian motion of a 0.5-m silica bead moving within an optical trap at a laser power of 6 mW in the specimen, obtained from a time series (partially shown in Fig. 1) of voltage readings from an interferometric detector (bandwidth 50 kHz). About 30 spectra from independent intervals of the original time series were averaged. The corner frequency is $f_c \approx 60$ Hz and the plateau power $S_0 = 0.028$ V²/Hz. In this case, the theoretical drag coefficient of the sphere (Eq. 20) was used to determine the trap stiffness, $\kappa = 1.7 \times 10^{-3}$ pN/nm, and to calibrate the response of the detector (32 nm/V).

and the drag coefficient γ of the particle is

$$\gamma = \frac{k_B T}{\pi^2 S_0 f_c^2}. \tag{18}$$

If γ is known from first principles (see later), κ can be calculated directly from the corner frequency f_c:

$$\kappa = 2\,\pi\gamma f_c. \tag{19}$$

By using Eq. (10), an attempt could be made to estimate $\kappa = k_B T/\mathrm{Var}(x)$ directly from the variance of the data set without examining the power spectrum. But this is risky because very low-frequency noise from drift, vibrations, or other sources will often artificially inflate $\mathrm{Var}(x)$. The advantage of plotting the power spectrum is that such effects are often easily recognizable; estimating S_0 and f_c generally gives a better value for κ. When κ has been determined from S_0 and f_c, a better estimate for $\mathrm{Var}(x)$ can, if needed, be calculated from Eq. (10). Similarly, instrumental noise at high frequencies may eventually cause the sloping spectrum to level off again, but this usually happens at an amplitude low enough not to affect the fit parameters.

C. Hydrodynamic Drag

It is often desirable to calculate the viscous drag coefficient γ of a particle from first principles, for example to compare with values estimated from a

thermal-noise power spectrum. Using Eq. (8), the object's free Brownian motion can also be predicted when γ is known. The hydrodynamic drag coefficient also needs to be known for calibrating trapping forces by sweeping the trap through the fluid and observing the particle displacement within the trap (Svoboda and Block, 1994a).

To calculate γ theoretically, a hydrodynamic problem must be solved. This is usually difficult, even when inertia is negligible at a low Reynolds number. The most important practical case was solved long ago and has a simple result: It is the Stokes drag on a small sphere far from any surface (Reif, 1965):

$$\gamma = 6\pi\eta a. \tag{20}$$

Here η is the dynamic viscosity of the solvent and a is the radius of the sphere.

There are many exact and approximate formulas giving γ for various particles in unbounded solutions (Happel and Brenner, 1983), and these apply to trapped particles as well. A complication often arises in microscopy experiments when the observed object is close to a sample chamber surface. For a particle close to a surface—at a distance similar to or less than its diameter (a)—the unbounded-solution drag coefficients are no longer correct and cannot be used to predict Brownian motion. Drag near a surface is due largely to shear between the particle and the wall, which is a different hydrodynamic situation from shear flow around a free particle. This remains true when flow is induced above a surface (so that velocity increases in proportion to the height above the surface); an unbounded-solution γ cannot be combined with a local velocity to obtain the drag force.

For a sphere in the vicinity of a surface, but still with $a/h < 1$, the correction to first order in a/h to Eq. (20) is

$$\gamma = 6\pi\eta a\left(1 + \frac{9}{16}\frac{a}{h}\right), \tag{21}$$

which applies to horizontal motion (parallel to the wall) with the sphere center at a height h. Moving vertically, toward or away from the wall, the factor in Eq. (21) becomes $(1 + (9/8)a/h)$. Equation (21) is known as the Lorentz formula (Happel and Brenner, 1983).

IV. Noise Limitations on Micromechanical Experiments

Micromechanical experiments measure forces and displacements produced by microscopic objects. Such measurements are typically done by monitoring small deformations or displacements $x_p(t)$ of an elastically suspended probe as it interacts with the object (Fig. 5). One example of such a probe is a particle in an optical trap in which, typically, probe motion is followed as a function of time. In atomic force microscopy (AFM) experiments, surfaces are imaged by scanning a sharply pointed, elastically suspended tip laterally across the surface and then converting the time series data of tip deflection into a spatial image. In an optical

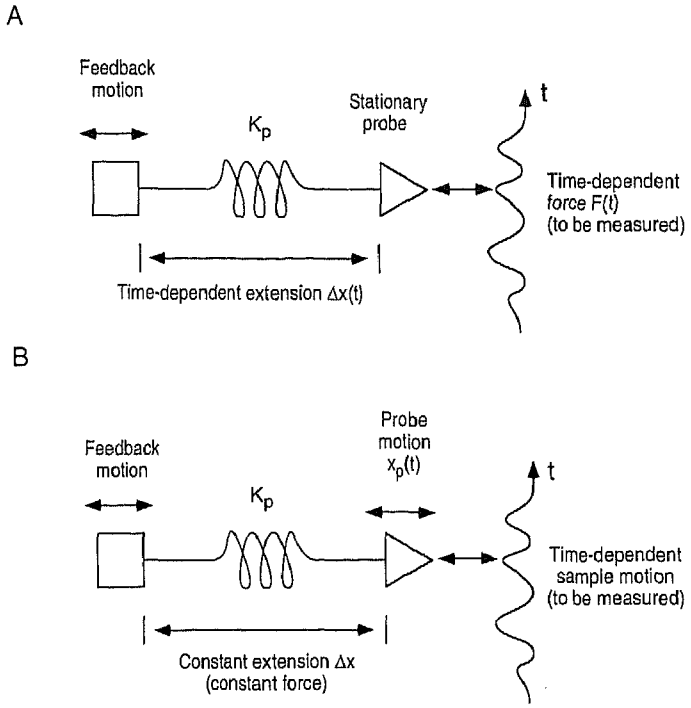

Fig. 5 Schematic representation of two prototypical micromechanical experiments. In an optical trap, the probe (triangle) is a trapped dielectric particle; the anchor point (square) represents the position of the center of the trap, which is controlled through feedback; and K_p represents the trap stiffness. In atomic force microscopy, the probe is the scanning tip; the anchor point is the base of the cantilever (controlled via feedback); and K_p represents the cantilever stiffness. The probe interacts with the sample through a force that, in general, changes with distance and time. (A) Position-clamp experiment to measure force. The absolute probe position is monitored with high precision, and the anchor point is moved to keep the probe stationary. From the changing distance between the probe and the anchor point (the probe strain), the changing force on the stationary probe can be deduced. (B) Force-clamp experiment to measure position. The probe position is again monitored, and the anchor point is moved to keep the probe strain, and thus the force on the probe, constant. The anchor motion then reflects how the sample moves under a fixed, constant force. The probe response is low-pass filtered by the dynamic response characteristics of the probe as described in Section IV, C of this chapter. If the probe is scanned along a surface (AFM), a constant-force contour, within the limitations of the probe dynamic response, is traced by the anchor motion.

trap, the displacement Δx of the particle away from the trap center $x_0(t)$ is measured (i.e., $\Delta x(t) = x_p(t) - x_0$ where $x_p(t)$ is the instantaneous position of the probe). In AFM, a tip displacement Δx represents the distortion of the elastic cantilever that supports the tip. In either case, we can call the relative displacement $\Delta x(t)$ the *probe strain.* If the stiffness K_p of the elastic element (the *probe stiffness*) has been calibrated, the suspension force on the probe is inferred as

$$F(t) = K_p \Delta x(t). \tag{22}$$

In scanned-tip AFM experiments and in some optical tweezers applications, feedback is used in conjunction with position detection; the anchor point of the "spring" holding the probe (e.g., the base of the cantilever or the center of the trap) can be moved quickly and precisely. There are then two prototypical experiments that can be performed—although actual experiments, or experiments done without feedback, may be intermediate between these two cases. In one case, force is measured (i.e., probe strain $\Delta x(t)$ is monitored) while feedback keeps the probe at an absolutely fixed position $x_p(t)$ = constant. This is a *position clamp* or isometric experiment. The other prototypical experiment measures probe motion at an absolutely constant force: Feedback keeps the probe strain Δx constant as the probe itself is moved by its interaction with the object. This is a *force clamp* or isotonic experiment. Force clamps and position clamps may seem to be unattainable idealizations, but, in fact, present technology, using piezoelectric actuators (in AFM) or acousto-optic or electro-optic modulators (with optical tweezers), can approximate ideal conditions quite well up to high frequencies. In both the position clamp and the force clamp, the anchor point of the probe assembly is moved by the feedback circuitry, but according to different criteria, keeping $x_p(t)$ constant in the first case and $\Delta x(t)$ constant in the second case. Different types of detectors are necessary for these two types of experiments. We next discuss how in these two cases the sensitivity of micromechanical measurements is limited by thermal noise.

A. Position-Clamp Experiments

First we consider pure force measurements by means of position clamping, in which one wants to measure a time-varying force signal $F_{sig}(t)$ on the probe. This would not normally be done with an AFM, but in an optical trap, for example, the force production of a molecular motor tied to a stationary load can be measured. When the varying force generated by the object begins to displace the probe, the equilibrium position $x_0(t)$ is quickly changed by moving the trap, changing the probe strain $\Delta x(t) = x_p - x_0(t)$ to balance the varying force and keep the probe at a fixed position, x_p. The total time-dependent force exerted on the probe is found from the observed $\Delta x(t)$:

$$F_{tot}(t) = K_p \Delta x(t). \tag{23}$$

Assuming that feedback control of the probe position is perfect, the fundamental limitation in measuring the force the object exerts on the probe comes from the presence of a white-noise thermal force that acts on the probe in competition with the force to be measured. From Eq. (12), the power spectrum of this thermal force is

$$S_F(f) = 4\gamma k_B T, \tag{24}$$

where γ is the frictional drag coefficient on the probe. In optical trapping, all friction comes from hydrodynamic drag on the trapped particle; in AFM, γ

includes all friction opposing the motion of the tip (i.e., drag on the tip and on the cantilever).

The practical implication of Eq. (24) is that the relative noise level can be decreased by low-pass filtering of the strain signal $\Delta x(t)$ with a cutoff frequency greater than the fastest rate of change in the signal. Because the force noise is distributed evenly over all frequencies, such filtering can increase the signal-to-noise ratio substantially. This argument assumes that the detection is fast enough to follow the force signal in the first place. How accurately can $F_{sig}(t)$ be determined at any particular time? As a concrete example, assuming fast enough detection, consider a force signal $F_{sig}(t)$ produced by a molecular motor: the slower the true signal varies, the better it can be resolved; the lower the permissible cutoff frequency of the low-pass filter, the more noise is removed. The remaining uncertainty $\Delta F(t) = F_{tot}(t) - F_{sig}(t)$ with a properly chosen filter frequency f_s corresponds, on average, to the integrated noise power below f_s, which is equal to the constant noise spectral density in Eq. (24) multiplied by the frequency range, 0 to f_s, passed by the filter,

$$\Delta F_{rms} = \sqrt{\overline{\Delta F^2}} = \sqrt{4\gamma k_B T f_s}. \tag{25}$$

Equation (25) states the fundamental resolution limit of a pure force measurement. It shows that the measurement can be optimized by either reducing the drag γ on the probe or keeping the rate of change of the true force signal f_s as low as possible (e.g., by scanning slowly with an AFM). Note that the stiffness of the elastic probe suspension is *not* relevant in principle. However, in practice, the noise in the strain detector electronics limits how small a strain in the probe can still be detected. Therefore, a softer probe allows measurement of both a smaller force change and a smaller absolute force. As a rule of thumb, the sensitivity of a detector is large enough or its noise contributions are low enough when the thermal motion of the probe can be detected. Increasing the sensitivity beyond this point brings no advantage.

Making sure that the force signal varies slowly, that is, reducing f_s in Eq. (25), may not always be possible. Nevertheless it is always advantageous to low-pass filter the signal to the lowest possible frequency. For static forces, $f_s = 0$ can, in principle, be measured to arbitrary precision with correspondingly long measurement times. In practice, however, measurements of static or very slowly varying forces are limited by drift in the apparatus, not by Brownian noise. In some cases the detection system is intrinsically slower than the variation of the signal. This typically happens when video recording and image processing is used for displacement detection. In that case it must be remembered that the detected position is a time average and may not reflect the true excursions of the probe.

B. Force-Clamp Experiments

Now we consider pure probe position measurements at constant force. The probe strain Δx is kept constant, corresponding to a constant suspension force

$F_{set} = K_p \Delta x$ on the probe that is balanced by the force of interaction with the sample. With an AFM it is possible, for example, to trace a surface or the shape of a biological macromolecule as defined by its constant-force contours. In an optical trap, the motion of a molecular motor under a constant load force can be followed.

We neglect, for the moment, viscous drag effects, which are treated in part C. In other words, we assume that the sample and the probe move very slowly. If thermal noise were absent, a force-clamp apparatus would allow a force value to be dialed in, and the probe would always exert *exactly* that force on the sample. The probe position $x_p(t)$ would exactly trace a constant-force contour of the object (in AFM) or follow exactly the motion of the motor protein under constant load (with optical tweezers). In reality, with thermal noise the force exerted by the elastic suspension of the probe (i.e., the optical trap or the cantilever) is balanced by the sum of sample interaction force and the fluctuating thermal force on the probe. The probe position $x_p(t)$ is then only an estimate for the true constant-load position corresponding to the dialed-in force.

There are two experimental goals that need to be distinguished at this point. Figure 6 illustrates the situation with a hypothetical interaction force profile between probe and sample. For example, this could be a plot of how the repulsive force increases when the tip of an AFM gets closer to a surface, or a plot of how the attractive force in the elastic linkage between a probe bead and a molecular motor increases with increasing distance. Thermal noise imposes dis-

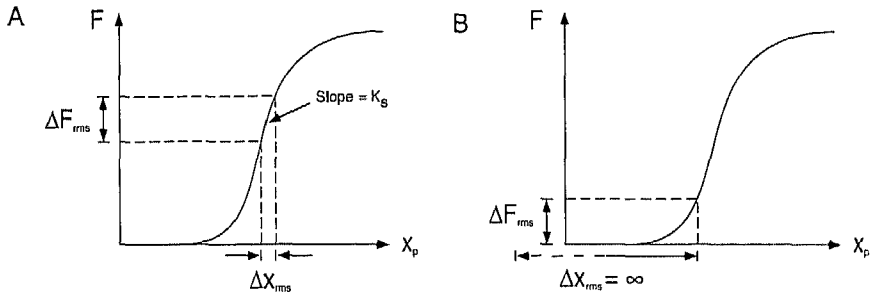

Fig. 6 Force-clamp experiments at high force and at low force (edge detection). The solid curve is an instantaneous force profile $F(x_p)$ as a function of probe position x_p. An uncertainty ΔF_{rms} in force measurement results from thermal forces on the probe. (A) The goal is to monitor changes in $F(x_p)$ with time, or equivalently to measure a spatial constant-force contour with a scanned probe (AFM). The apparatus is operating in a constant-force mode at values F_{set} well above the force uncertainty $F_{set} >> \Delta F_{rms}$. The force uncertainty translates, via the slope K_s of $F(x_p)$, into an uncertainty in locating the position $x(F_{set})$ on the force profile corresponding to the set force. The force resolution ΔF_{rms} of the apparatus is given by Eq. (27). (B) Locating the "edge" of a profile in the least invasive manner (i.e., using the smallest possible force). In any real system the interaction force will smoothly approach zero at some distance. The smallest possible set force is $F_{set} \approx \Delta F_{rms}$. If F_{set} approaches ΔF_{rms} the position uncertainty diverges to infinity.

tinct limitations in two experimental situations: (a) It limits the accuracy with which a high-force spatial response can be determined, and (b) it sets a minimum force at which a spatial response can be obtained at all. We consider each of these cases in turn.

1. Displacement Measurements with Force Clamp at Large Forces

To be specific, one might want to challenge a molecular motor with a load close to its stalling force or to image the underlying substrate of an AFM sample. The displacement response to a strong force may, of course, include some deformation of the object under study. Note that the quantity being recorded is always the probe position $x_p(t)$ for the set interaction force F_{set}. Which property of the sample this reflects varies from case to case. It could, for example, report conformational changes in a motor protein in the case of our optical tweezers example, or local differences in the surface chemistry for the AFM example. In any case, what we mean by "large" force is that F_{set} is large compared to the root-mean-square thermal force on the probe $F_{set} >> \Delta F_{rms}$ (see Eq. 25). The position uncertainty in the experiment is caused by the force uncertainty ΔF_{rms} (Fig. 6A). If the local stiffness of the probe sample interaction is K_s (i.e., the local slope of F vs. x in Fig. 6), then

$$\Delta x_{rms} = \frac{\sqrt{4\gamma k_B T f_s}}{K_s}. \tag{26}$$

This is the fundamental limit of a pure position measurement at a relatively large constant force. Again, the stiffness of the trap or cantilever does *not* enter directly, but, instead, the characteristics of the force between probe and object are determining the error. For example, in measuring the displacement $x_p(t)$ caused by the action of a molecular motor, Eq. (26) shows that the uncertainty Δx_{rms} can be very small if the stiffness K_s of the bead motor linkage is high. The thermal noise can be further reduced by decreasing the drag coefficient of the probe. It is also still true that static displacements against a finite load can be measured better the longer one takes to measure them (reducing f_s). In practice, though, mechanical drift is encountered again at long times.

2. Edge Detection

In some situations it is necessary to detect the edge of a force profile without disturbing the object. This is crucial, for example, in imaging soft biomolecules by AFM, when it is desirable to follow the lowest possible force contour. This situation is illustrated in Fig. 6B, in which the object force $F_{obj}(t)$ is shown as a curve. In any real system the interaction force between probe and sample will smoothly approach zero at some distance as shown in the figure. Again neglecting viscous drag, the suspension force on the probe F_{set} is always balanced by both

the sample–probe interaction force and the random thermal force $\Delta F(t)$ given by Eq. (25): $F_{set} + \Delta F(t) + F_{obj}(t) = 0$. The thermal noise now determines the lowest force contour that can be followed. Consider, for example, how the feedback system operates for an AFM probe close to a repulsive surface. Assume that a thermal $\Delta F(t)$ pushes against the probe in the same direction as the surface. The feedback will move the probe farther away from the surface, decreasing $F_{obj}(t)$ to compensate. Now, if F_{set} is so low that $F_{set} + \Delta F(t)$ can become negative, the feedback will try to move the probe infinitely far away from the surface (i.e., it cannot compensate). In practice, this means that to locate the "edge" of a force profile, at least a force $F_{set} \approx \Delta F_{rms} = \sqrt{4\gamma k_B T f_s}$ must be applied.

For noise reduction, as in a position-clamp experiment, the primary goals are to reduce the drag on the probe and the filter frequency f_s. Surprisingly, probe stiffness again is not a direct consideration in avoiding sample deformation. In practice, however, detector resolution in the feedback circuit may become limiting, in which case a lower force clamp is possible with a less stiff probe such as a softer cantilever.

C. Dynamic Response of the Probe Interacting with a Sample

There is an important dynamic limitation for force-clamp experiments that we neglected so far and which is closely related to the preceding noise discussion. Even if feedback is perfect and the suspension force is held constant, the probe cannot respond instantaneously to the motion of the sample because of the viscous drag γ on the probe. For example, if an AFM scan is made at too high a scan rate, the probe will not follow a compliant surface, but will simply plow through a nearly constant height, yielding little information. Alternatively, if a motor protein performs a fast conformational change, the bead that holds the motor cannot instantaneously follow the change. Consequently, a force clamp cannot, in principle, follow motion perfectly if the probe has any drag at all. The probe motion is a low-pass filtered version of the object motion, and the force on the object deviates from the set value.

Assume that by using a probe with no drag ($\gamma = 0$), an "ideal" constant-force probe motion could be measured; call this $x_{p0}(t)$. In an actual measurement with probe motion $x_p(t)$, however, the drag force on the probe is $-\gamma dx_p(t)/dt$, which causes the actual motion to be different from $x_{p0}(t)$. If the local stiffness of the probe–object interaction is K_s, drag force is balanced by an additional sample deformation force, which is $K_s\,(x_p(t) - x_{p0}(t))$. This balance can be written as

$$\gamma \frac{d}{dt} x_p(t) + K_s x_p(t) = K_s x_{p0}(t). \tag{27}$$

In a procedure similar to that following Eq. (11), it is found from Eq. (27) that the power spectrum $S_x(f)$ of $x_p(t)$ is related to the power spectrum $S_{x0}(f)$ of the ideal signal $x_{p0}(t)$ by

$$S_x(f) = \frac{f_{ps}^2}{(f_{ps}^2 + f^2)} S_{x0}(f). \tag{28}$$

The signal is cut off above a characteristic probe-sample frequency $f_{ps} = K_s/2\pi\gamma$. This means that signal frequencies higher than f_{ps} will be suppressed by the probe response and will be unmeasurable in practice.

For example, in experiments measuring motor protein forces, the stiffness K_s of the motor-bead linkage may be variable, between 0.01 and 0.1 pN/nm (Coppin *et al.*, 1996; Kuo *et al.*, 1995; Meyhofer and Howard, 1995; Svoboda and Block, 1994b; Svoboda *et al.*, 1993), which for 0.5-μm beads implies a cutoff frequency on the order of 1 kHz. In contrast, AFM probes against protein surfaces, which typically have elastic moduli of several GPa (Gittes *et al.*, 1993), show effective spring constants K_s on the order of 10^2pN/nm, which for a low-drag probe could lead to very high cutoff frequencies.

V. Sources of Instrumental Noise

Optical trapping experiments are most often combined with some form of light microscopy, so that the laser and the special optics required are added to a commercial microscope or integrated into a custom-built microscope (Kuo and Sheetz, 1993; Molloy *et al.*, 1995; Simmons *et al.*, 1996; Smith *et al.*, 1996; Svoboda and Block, 1994a; Svoboda *et al.*, 1993). Nanometer-scale position detection, usually of a trapped latex or silica bead, is commonly the primary measurement. From the displacement, appropriate calibration of the trapping force provides a measure for the force exerted on the bead. Several sources of instrumental noise, depending on the specific detection method, will affect the primary displacement measurement and limit both its spatial and temporal resolution.

It is often easiest to use an existing standard video system to determine bead position from its video image via fluorescence or a contrast-enhancing transmitted-light imaging method such as phase contrast or differential interference contrast microscopy (DIC). In this case, temporal resolution is limited to the video half-frame rate of 60 or 50 Hz, depending on the video system used. This usually is not sufficient to resolve dynamic processes on the level of single molecules. Spatial resolution is limited, in a complicated way, by the optics, the camera, the video storage device, the image processing method, and so forth (Gelles *et al.*, 1988; Inoue, 1986; Schnapp *et al.*, 1988). In practice it is very hard to achieve a position resolution as low as 10–20 nm for an object such as a 0.5-μm silica bead. For these reasons, most quantitative experiments are performed using nonimaging detection systems based on photodiodes. We discuss these systems in more detail.

A. Noise from Electronics

The amplifier design to be used with photodiodes depends on the conditions of the experiment. Good introductions can be found in the literature (Horowitz

and Hill, 1989; Sigworth, 1995) and in photodiode manufacturer's catalogs [e.g., UDT Sensors, Inc. (Hawthorne, Ca), Advanced Photonics, Inc. (Camarillo, Ca), Hamamatsu (Hamamatsu City, Japan)]. If speed and linearity are important, and if the light levels are not extremely low, photoconductive operation with a reverse bias is best (Figure 7A). A low-noise operational amplifier acts as a current-to-voltage converter, so that the photodiode is operated as a pure current source. We now discuss sources of noise for this case. The responsivity of silicon photodiodes varies between 0.2 and 1.0 A/W for light with wavelengths between 350 and 1100 nm, with a maximum at about 1000 nm. Light levels as low as pW can be detected, at the cost of poor time resolution (i.e., low bandwidth; see later). In practice, intensities more than approximately 100 μW in typical optical-tweezers experiments result in a signal-to-noise ratio of better than 1×10^5 at a bandwidth of 100 kHz. At the high end, the maximum intensity that can be

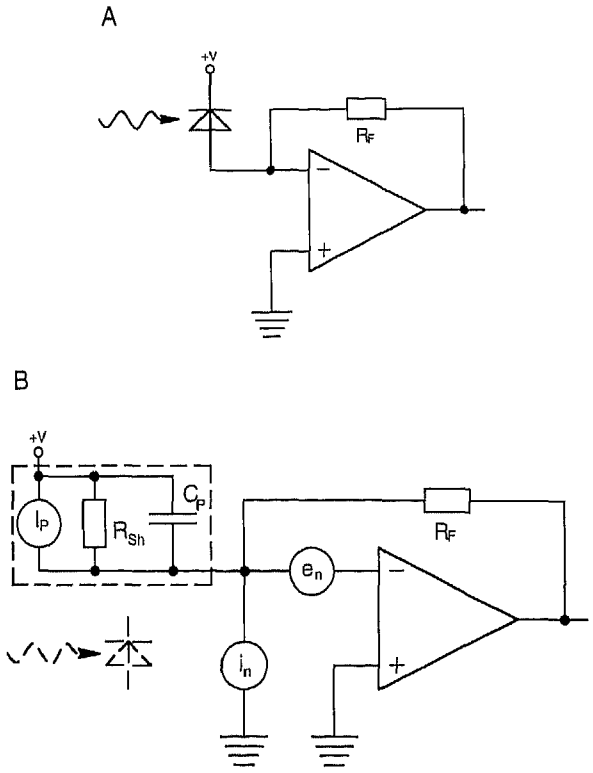

Fig. 7 (A) A typical circuit diagram for operating a photodiode in photoconductive mode with a reverse bias (current-to-voltage converter). (B) Equivalent circuit for the purpose of noise discussion. Noise sources that in reality are internal to the operational amplifier are represented by an equivalent voltage source e_n and a current source i_n acting at the inputs to the op-amp. The photodiode is replaced by an equivalent circuit including the junction capacitance, the shunt resistance, and an ideal current source.

measured depends on both the area of the detector and the width of the light beam. Deviations from linearity, to maximum intensities of approximately 1 mW/cm^2, are typically below 5%, but by 10 mW/cm^2 the response is strongly nonlinear. Linearity is improved at high light levels by using a large reverse bias in photoconductive operation.

Most of the noise sources discussed here are, at least approximately, white noise (i.e., the noise power spectrum of each is approximately constant for all frequencies). If the bandwidth (i.e., the Nyquist frequency) is given, each of these noise contributions can be calculated as a mean-squared noise current and added together—assuming they are statistically independent—to give the total mean-squared noise current. The square root of this quantity can then be compared to the photocurrent to obtain a relative noise contribution. Figure 7B shows an equivalent model circuit highlighting the noise sources discussed in the following.

1. Shot Noise

Photons are absorbed in the diode, creating electron-hole pairs and, eventually, a flow of current in the external circuit. Measuring this current amounts to counting elementary charges, which like other random counting processes (Poisson processes) results in a statistical variance equal to the number of counts, $\overline{\Delta n^2} = \bar{n}$. This gives rise to a counting noise, known as shot noise, as follows (Horowitz and Hill, 1989). Suppose there is an average photocurrent I_p, which we want to measure with a certain time resolution Δt (i.e., we count the number of electrons arriving within each sampling window Δt). As discussed earlier, a sampling time Δt corresponds to a bandwidth (Nyquist frequency) of $B = 1/(2\,\Delta t)$. The number of electrons counted in each bin, and therefore the variance in the number of counts, is $\overline{\Delta n_e^2} = \bar{n}_e = \Delta t I_p/q_e$, where q_e is the elementary electronic charge of 1.6×10^{-19} C, and I_p is the photocurrent. Therefore the variance in the current (Fig. 8) is

$$\overline{\Delta I_S^2} = \frac{q_e^2 \overline{\Delta n_e^2}}{\Delta t^2} = 2 q_e I_p B. \tag{29}$$

This result shows that shot noise is a white noise: It has a constant spectral density of $2q_eI_p$. The minimal current I_p entering this equation at the lowest light levels is the dark current of the photodiode, which for low-noise diodes is approximately 50 nA (for a 100-mm^2 diode at 10 V bias voltage). Shot noise is usually the dominating noise source if the electronics are designed carefully, using low-noise components. As an example, assume a photocurrent of I_p = 5 mA, corresponding to a light intensity of 12.5 mW at a responsivity of 0.4 mA/mW. With a bandwidth of B = 100 kHz, the root-mean-square shot-noise current from Eq. (29) is I_s = 12.6 nA, a relative contribution of 2.5 ppm in the 5 mA photocurrent.

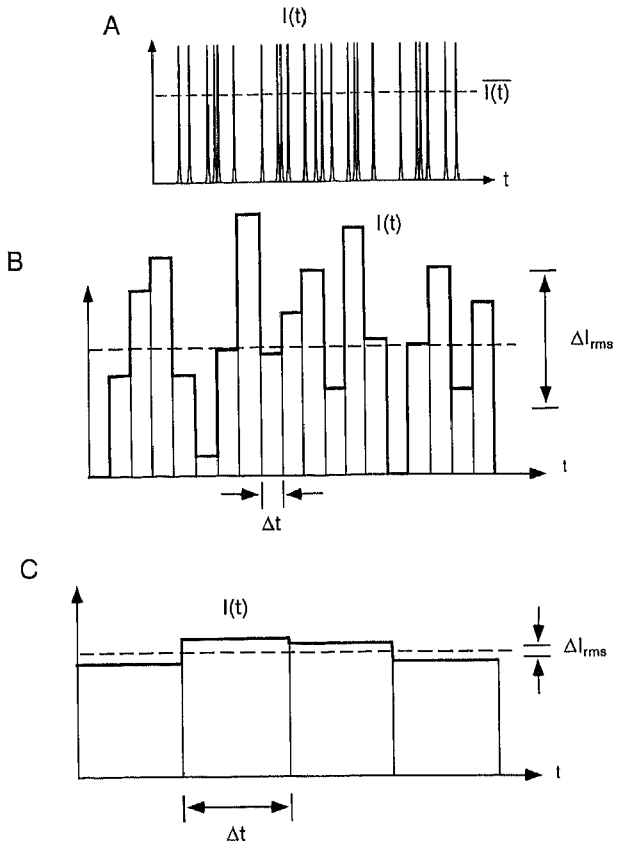

Fig. 8 The origin of shot noise. (A) A current I(t) due to the independent passage of elementary charge carriers through a point in the circuit (such as through the photodiode p-n junction) consists of a series of very narrow spikes. (B) Measuring current with a small window size Δt, and thus a large Nyquist frequency $f_{Nyq} = 1/(2\Delta t)$, means that a small number of spikes are counted in each sampling time. The measured current thus has a large variance, which is the shot noise superposed on the DC current value. (C) Measuring current with a larger window size, and thus a smaller Nyquist frequency, means that proportionally more charges are counted in each sampling time. The random noise superposed on the DC current value is smaller. As shown in this chapter, the variance of this random noise is proportional to the Nyquist frequency.

2. Johnson Noise

Any resistor produces noise, called Johnson noise, through the thermal motion of its electrons. This noise appears as a fluctuating voltage across the terminals of the resistor, or as a fluctuating current if the terminals are connected by other circuitry (Horowitz and Hill, 1989). This random voltage is exactly analogous to the random force in Brownian motion, and the voltage power spectrum S_v is given by Eq. (16) except that the drag coefficient is replaced by the resistance R: $S_v = 4k_BTR$. Because S_v is a constant, Johnson noise is white noise. In our

circuit (Fig. 7B), the shunt resistance R_{shunt} and the feedback resistor R_{Fbk} each contribute a mean-squared current that is their mean-squared Johnson voltage divided by the respective R^2. Multiplying by bandwidth B, gives the mean-squared Johnson current:

$$\overline{\Delta I_J^2} = \frac{4k_B TB}{R}. \tag{30}$$

Assuming R_{shunt} = 5 MΩ and R_{Fbk} = 1 kΩ, and a bandwidth of 100 kHz will give root-mean-square noise currents of $\Delta I_J(R_{shunt})$ = 18pA, and $\Delta I_J(R_{Fbk})$ = 1.3 nA respectively, both smaller than the shot noise. Also, depending on material and construction, resistors produce some excess noise in addition to their Johnson noise. It is important to choose low-noise resistors, typically metal-film resistors, for at least the input stages of the amplifier.

3. Amplifier Noise

Operational amplifiers produce their own noise because of the shot noise and resistor noise that originate from their internal elements. It is common (e.g., in data sheets for op-amps) to express these noises as input equivalent voltage and current, that is, voltage and current at the input of an ideal op-amp that would produce the same noise at the output (Horowitz and Hill, 1989), as shown in Figure 7B. Data sheets for op-amps usually state an "equivalent root-mean-square input noise voltage" e_n and an "equivalent root-mean-square input noise current" i_n, which actually are the square roots of the power spectral densities of noise voltage and current and must be multiplied by the bandwidth B to obtain the actual root-mean-square quantities. Because in our application we want to compare all noise contributions to the photocurrent, we need to convert the amplifier noise voltage into a current using the feedback resistor R_{Fbk} and the photodiode capacitance C_P and add it to the input current noise i_n^2 to find the total amplifier noise:

$$\overline{\Delta I_{amp}^2} = \left[\frac{1}{R_{Fbk}^2} + (2\pi f)^2 C_P^2\right] e_n^2 B + i_n^2 B. \tag{31}$$

Taking data from a typical appropriate operational amplifier, AD743 (Analog Devices, Norwood, MA), $e_n \approx 3$ nV/Hz$^{1/2}$, i_n = 6.9 fA/Hz$^{1/2}$, ignoring the slight frequency dependence of the noise voltage, assuming R_{Fbk} = 1 kΩ, C_p = 300 pF, and again assuming a bandwidth of 100 kHz, we calculate ΔI_{amp} = 1.0 nA. This an upper limit because we just used the smallest reactance of the diode (at 100 kHz) for the whole frequency range. Compared to the shot noise (12.6 nA, in our example) op-amp noise currents are negligible, although this may not be the case if low-quality components are used, or if the band width must be higher. The next stages in amplification usually contribute less noise than the input stage.

The relative error can, of course, change dramatically when the difference between two photodiode signals is computed. This is usually the case in position detection using, for example, a quadrant diode. It is then more meaningful to express the noise level as a minimal measurable displacement. In the displacement detection system in our laboratory, we end up with electronic noise corresponding to about 0.5Å in displacement of a 0.5-μm silica bead at 100 kHz bandwidth.

As a final stage of the electronic detection, if the measurements eventually are read into a computer, digitization errors need to be considered. The resolution of an analog-to-digital converter (ADC) is given in bits: A 16-bit ADC translates the maximal analog voltage for which it is designed (typically 10 V) into the integer number $2^{16} = 65{,}536$. Besides simple rounding error, imperfections in the circuitry usually cause the least significant bit to fluctuate between 1 and 0. If this error is independent for each sampled voltage point, the result will be white noise with root-mean-square variation of $1/65{,}536 \approx 15$ ppm, but spread out to the Nyquist frequency. Bandwidth reduction in general will decrease this error. However, ADC noise is complicated and sometimes is not even limited to the last bit, depending on the type of converter and the computer environment. In case of doubt it is best to measure the converter noise directly. ADCs with relatively few bits or an input signal not using the full dynamic range of the ADC obviously present problems.

B. Other Noise Considerations

With enough light intensity, as described earlier, photodiode detection can be used to monitor the motion of μm-size beads, with Å resolution, at bandwidths up to 100 kHz. A laser is commonly used to achieve sufficient intensity focused on a bead. In using optical tweezers, this laser can be the trapping laser itself or a separate laser. The advantage of using the trapping laser is that the detection system is intrinsically aligned with the trap and a relative displacement is measured. If absolute position needs to be measured while the trap is moved, a separate laser is needed. By using a laser focused on the trapped object, a number of new noise problems are created. Lasers show fluctuations in laser power, beam pointing, and frequency. Intensity fluctuations are usually a few percent of the maximal power and are not critical as long as the laser is operated at a relatively high power and intensity regulation for trapping or detection is performed farther down the line (e.g., with polarization optics). Most lasers are also extremely sensitive to backreflections, which can cause large-amplitude intensity oscillations. The most efficient but costly way to avoid these is to use a Faraday-effect type of optical isolator (Optics for Research, Caldwell NJ; Conoptics Inc., Danbury CT; Electro-Optics Technology, Inc., Traverse City MI). Alternative low-cost approaches are (a) placing the first reflecting surface at a distance from the laser that is larger than the coherence length of the laser; (b) Using a neutral density filter (tilted to the beam) to attenuate the transmitted and the back-reflected beam, which is only practical if there is laser power to spare; and (c) using

the combination of a linear polarizer and quarter-wave plate, which produces circularly polarized light if the polarizer is oriented at 45° to the fast axis of the quarter-wave plate. Light back-reflected off a mirror has the sense of its circular polarization inverted and is blocked by the polarizer after being converted back to linearly polarized light by the quarter-wave plate. In practice this method is limited in its effectiveness because back-reflections can have phase changes other than what a plane mirror produces at normal incidence.

Beam-pointing fluctuations are a more serious problem. They are caused mainly by changing thermal gradients inside the laser. Different types of lasers show different amounts of these fluctuations. Large-frame noble gas lasers usually show fewer fluctuations than solid state lasers (Siders *et al.*, 1994). For diode lasers, data were not available from manufacturers. Among the solid state lasers, which are most often used for optical trapping, the crystalline substrates vary in thermal conductivity. Thermal lensing, caused by thermal gradients in the laser rod, is in some designs used intentionally for gain increase. Neodymium : yttrium lithium fluoride (Nd:YLF) has a large thermal conductivity and therefore less beam-pointing instabilities than neodymium:yttrium aluminum garnet (Nd:YAG). It is best to request detailed information from design engineers at the manufacturer. Beam-pointing instabilities for solid state lasers are typically up to 50 μrad, and the beam usually does not pivot around a fixed point. For trapping, the beam usually is expanded by a factor of about 5, which decreases angular fluctuations by the same factor. Assuming a typical focal length of 1.5 mm in a high-magnification microscope objective, a laser with pointing fluctuations of 10 μrad in the back focal plane of the objective will cause lateral fluctuations of the trap by about 15 nm. Using this laser for position detection would thus severely limit the resolution. The pointing fluctuations are typically quite slow, on the order of 1 Hz and slower, so that fast displacements still can be detected with better resolution. Single-mode polarization-preserving optical fibers have been used to stabilize the beam (Denk and Webb, 1990; Svoboda *et al.*, 1993). The reduction in beam-pointing fluctuations can be on the order of 10-fold, but fibers introduce their own noise problems, acting as microphones for vibrations and changing their output mode pattern with small temperature fluctuations. We find in our laboratory that even with maximal precautions, the output of such a single-mode fiber still has beam-pointing fluctuations on the order of 10 μrad. Depending on the specific experimental situation, this can be unacceptable. Fibers are also costly, produce coupling losses, and need careful alignment. Therefore, fibers do not always solve the problem. Active feedback-controlled beam-pointing stabilization is possible and may well be the best way to increase resolution for slow processes (Grafstrom *et al.*, 1988; Siders *et al.*, 1994).

Care also must be taken to prevent additional beam-pointing noise by beam-steering devices that are used to move the laser trap into the field of view of the microscope. Galvanometer mirrors, for example, exhibit thermal jitter in the range of 10 to 100 μrad. If acousto-optic modulators (AOM) are used to control beam pointing, frequency stability of the controller is crucial. Piezoelectrically

actuated mirrors show creep and hysteresis effects that need to be controlled by feedback circuitry.

Finally there are always vibrations and drifts in the microscope, in the laser, and in the detection setup. Building vibrations can be cut off by using an optical bench on vibration-isolated supports. These devices eliminate vibrations faster than a few Hz, but still let slow vibrations pass. Acoustic vibrations are also coupled through the air, making it necessary to eliminate strong noise sources.

VI. Conclusions

We have provided a basic tutorial on noise issues in micromechanical experiments that should be helpful for the nonspecialist in designing experiments. Single-molecule experiments are difficult, and it may save a lot of time to be aware of fundamental facts as well as tricks of the trade that can often be unexpected and counterintuitive. Power spectral analysis is a powerful method much used in physics, but often not appreciated in biological applications. There are some universal recipes to reduce noise in micromechanical experiments, such as low-pass filtering and reducing viscous drag on the probe, but probe stiffness does not play a direct role. For fast motions, viscous drag forces on the probe need to be taken into account, with the consequence that a true constant force experiment is not possible in principle. Finally, we have presented a selection of instrumental design criteria that should be of particular relevance to quantitative optical trapping experiments.

Acknowledgements

We acknowledge detailed discussions with Winfried Denk, who first pointed out that force resolution is independent of probe stiffness in micromechanical measurements, as well as with Karel Svoboda and Winfield Hill. We thank Winfried Denk, Winfield Hill, Karel Svoboda, and Manfred Radmacher for their comments on the manuscript. We acknowledge support from the National Science Foundation (grant #BIR-9512699), the Whitaker Foundation, and the donors of the Petroleum Research Foundation, administered by the American Chemical Society.

References

Ashkin, A. (1992). Forces of a single-beam gradient laser trap on a dielectric sphere in the ray optics regime. *Biophys. J.* **61**, 569–582.

Ashkin, A., and Gordon, J. P. (1983). Stability of radiation-pressure particle traps: An optical Earnshaw theorem. *Optics Lett.* **8**, 511–513.

Ashkin, A., Dziedzik, J. M., Bjorkholm, J. E., and Chu, S. (1986). Observation of a single-beam gradient force optical trap for dielectric particles. *Optics Lett.* **11**, 288–290.

Betzig, E., and Chichester, R. J. (1993). Single molecules observed by near-field scanning optical microscopy. *Science* **262**, 1422–1428.

Bobroff, N. (1986). Position measurement with a resolution and noise-limited instrument. *Rev. Sci. Instrum.* **57**, 1152–1157.

Coppin, C. M., Finer, J. T., Spudich, J. A., and Vale, R. D. (1996). Detection of sub-8-nm movements of kinesin by high-resolution optical-trap microscopy. *Proc. Natl. Acad. Sci. USA* **93,** 1913–1917.

Denk, W., and Webb, W. W. (1990). Optical measurement of picometer displacements of transparent microscopic objects. *Appl. Optics* **29,** 2382–2391.

Funatsu, T., Harada, T., Tokunaga, M., Saito, K., and Yanagida, T. (1995). Imaging of single fluorescent molecules and individual ATP turnovers by single myosin molecules in aqueous solution. *Nature* **374,** 555–559.

Gelles, J., Schnapp, B. J., and Sheetz, M. P. (1988). Tracking kinesin-driven movements with nanometre-scale precision. *Nature* **331,** 450–453.

Gittes, F., Mickey, B., Nettleton, J., and Howard, J. (1993). Flexural rigidity of microtubules and actin filaments measured from thermal fluctuations in shape. *J. Cell Biol.* **120,** 923–934.

Grafstrom, S., Harbarth, U., Kowalski, J., Neumann, R., and Noehte, S. (1988). Fast laser beam position control with submicroradian precision. *Optics Comm.* **65,** 121–126.

Happel, J., and Brenner, H. (1983). "Low Reynolds Number Hydrodynamics: With Special Applications to Particulate Media." 1st ed. (M. Nijhoff, ed.) The Hague, Boston, Hingham, Massachusetts: Kluwer.

Horowitz, P., and Hill, W. (1989). "The Art of Electronics." 2nd ed. Cambridge (England), New York: Cambridge University Press.

Inoue, S. (1986). "Video Microscopy." New York: Plenum Press.

Kuo, S. C., and Sheetz, M. P. (1993). Force of single kinesin molecules measured with optical tweezers. *Science* **260,** 232–234.

Kuo, S. C., Ramanathan, K., and Sorg, B. (1995). Single kinesin molecules stressed with optical tweezers. *Biophys. J.* **68,** 74S.

Landau, L. D., Lifshits, E. M., and Pitaevskii, L. P. (1980). "Statistical Physics." Oxford, New York: Pergamon Press.

Meyhofer, E., and Howard, J. (1995). The force generated by a single kinesin molecule against an elastic load. *Proc. Natl. Acad. Sci. USA,* **92,** 574–578.

Molloy, J. E., Burns, J. E., Sparrow, J. C., Tregear, R. T., Kendrick-Jones, J., and White, D. C. (1995). Single-molecule mechanics of heavy meromyosin and S1 interacting with rabbit or Drosophila actins using optical tweezers. *Biophys. J.* **68,** 298S–303S.

Press, W. H. (1992). "Numerical Recipes in C: The Art of Scientific Computing." 2nd ed. Cambridge, New York: Cambridge University Press.

Radmacher, M., Fritz, M., and Hansma, P. K. (1995). Imaging soft samples with the atomic force microscope: Gelatin in water and propanol. *Biophys. J.* **69,** 264–270.

Reif, E. (1965). "Fundamentals of Statistical and Thermal Physics." New York: McGraw-Hill.

Rugar, D., and Hansma, P. (1990). Atomic force microscopy. *Physics Today* **43,** 23–30.

Sase, I., Miyata, H., Corrie, J. E., Craik, J. S., and Kinosita, K., Jr. (1995). Real-time imaging of single fluorophores on moving actin with an epifluorescence microscope. *Biophys. J.* **69,** 323–328.

Schnapp, B. J., Gelles, J., and Sheetz, M. P. (1988). Nanometer-scale measurements using video light microscopy. *Cell Motil. Cytoskeleton* **10,** 47–53.

Siders, C. W., Gaul, E. W., Downer, M. C., Babine, A., and Stepanov, A. (1994). Self-starting femtosecond pulse generation from a Ti:sapphire laser synchronously pumped by a pointing-stabilized mode-locked Nd:YAG laser. *Rev. Sci. Instrum.* **65,** 3140–3144.

Sigworth, F. J. (1995). Electronic design of the patch clamp. *In* "Single-Channel Recording" (B. Sakman and E. Neher, eds.), 2nd ed., pp. 95–127. New York: Plenum Press.

Simmons, R. M., Finer, J. T., Chu, S., and Spudich, J. A. (1996). Quantitative measurements of force and displacement using an optical trap. *Biophys. J.* **70,** 1813–1822.

Smith, S. B., Cui, Y. J., and Bustamante, C. (1996). Overstretching B-DNA—the elastic response of individual double-stranded and single-stranded DNA molecules. *Science* **271,** 795–799.

Svoboda, K., and Block, S. M. (1994a). Biological applications of optical forces. *Annu. Rev. Biophys. Biomol. Struct.* **23,** 247–285.

Svoboda, K., and Block, S. M. (1994b). Force and velocity measured for single kinesin molecules. *Cell* **77,** 773–784.

Svoboda, K., Schmidt, C. F., Schnapp, B. J., and Block, S. M. (1993). Direct observation of kinesin stepping by optical trapping interferometry. *Nature* **365,** 721–727.

Thomson, N. H., Fritz, M., Radmacher, M., Cleveland, J. P., Schmidt, C. F., and Hansma, P. K. (1996). Protein tracking and detection of protein motion using atomic force microscopy. *Biophys. J.* **70,** 2421–2431.

Wax, N. (1954). "Selected Papers on Noise and Stochastic Processes." New York: Dover.

Yin, H., Wang, M. D., Svoboda, K., Landick, R., Block, S. M., and Gelles, J. (1995). Transcription against an applied force. *Science* **270,** 1653–1657.